Journal of Nanofluids
Vol. 7, pp. 246–257, 2018
(www.aspbs.com/jon)

ARTICLE

Influence of Silver Nanoparticles Morphologies on Density, Viscosity and Thermal Conductivity of Silver Nanofluids and Silver IoNanofluids

V. S. Patil[1], A. Cera-Manjarres[1], D. Salavera[1], C. V. Rode[2], K. R. Patil[2], and A. Coronas[1,*]

[1]*Group of Research on Applied Thermal Engineering–CREVER, Department of Mechanical Engineering, Universitat Rovira i Virgili. Av. Països Catalans 26, 43007, Tarragona, Spain*
[2]*CSIR-National Chemical Laboratory, Pashan Pune 411008, Maharashtra, India*

This paper explores the consequence of silver nanoparticles morphology (nanowires, nanoplates, and nanospheres) on density, viscosity and thermal conductivity of nanofluids and IoNanoFluids. Nuclear magnetic resonance spectroscopy results reveal that hydroxyl group in cation relates to silver nanoparticle surface of silver IoNanoFluid. Effect on bonding of silver nanoparticles after solvation in an ionic liquid was investigated with Infrared spectroscopy. UV-Visible spectroscopy analysis observed variations in color and optical properties of silver IoNanoFluids compared with nanofluids. Structural and morphological characterization of silver nanofluids and silver IoNanoFluids were carried out with Scanning electron microscopy and Transmission electron microscopy techniques. The presence of silver nanoparticles from the aqueous phase of nanofluids to viscous ionic liquid phase was confirmed by X-ray photoelectron spectroscopy and Energy dispersive analysis. The thermal stability study unveils that Choline bis(trifluromethylsulfonyl)imide ionic liquid, and its derived silver IoNanoFluids, are more stable than silver nanofluids. There was no considerable impact was observed for the silver nanoparticles morphology on the density of IoNanofluids. Moreover, two-dimensional silver structures raise the viscosity further compare to other two morphologies of silver nanoparticles in a base ionic liquid. Among all three studied morphologies, silver nanowires influence additional in the enhancement of thermal conductivity for silver nanofluids and IoNanoFluids. Enhanced thermal conductivity and reduced viscosity of silver nanowires based IoNanoFluid sorts this fluid as a potential heat transfer fluid.

KEYWORDS: Silver Nanoparticles, Choline Bis(trifluromethylsulfonyl)imide, Ionic Liquids, IoNanofluids, Density, Thermal Conductivity, Viscosity.

1. INTRODUCTION

The heat transfer fluids play an important role in heat transfer based applications designed for heat recovery, solar energy, automotive industry, etc. The hunt for novel fluids with improved thermal properties is a challenge considering their impact on economics in designing of these heat transfer based technologies.[1] A way to improve the thermal properties of the conventional heat transfer fluids is the addition of nanosized materials.[2–9] Nevertheless, fluids like water, ethylene glycol and synthetic oil containing nanoparticles of different materials utilized as a heat transfer media have some drawbacks, like low operating temperature, high vapor pressure, and poor thermal stability.[10–12] To overcome these problems, some researchers propose the use of ionic liquids (ILs) as an alternative. This can be employed as a new generation of heat transfer fluids due to their low vapor pressure, improved thermal conductivity and high temperature operating conditions.[13] Even the addition of a small fraction of nanoparticles into the ILs displays an improvement in thermal properties of the ILs makes it possible to use them in small volume heat exchangers and microchannels.[14] Besides the improvement in the thermophysical properties of heat transfer fluids, the designed or developed materials must be more eco-friendly.

In this paper, we propose a new class of IoNanoFluids (INF's) as novel heat transfer fluids, based on Choline-based ILs with silver nanoparticles. On the one hand, the presence of hydroxyl group improves the biodegradability of the IL,[15,16] and besides that, silver (Ag) is a well-known metal for the high thermal conductivity, showing an enhancement of this property in conventional solvents.[17] For the development of a new class

*Author to whom correspondence should be addressed.
Email: alberto.coronas@urv.cat
Received: 20 June 2017
Accepted: 10 August 2017

of INF's for heat transfer applications, it is necessary to investigate their essential properties such as density, viscosity and thermal conductivity,[18] and to explore the effect of the variation in particle morphology in fluids on their thermophysical properties. Even though the dispersing materials with higher thermal conductivity and with the variety of available ILs, it is difficult to disperse the desired nanoparticles in the desired base ILs due to high viscous nature of ILs.[19] Here, we follow a protocol based on phase transfer for dispersion of silver nanoparticles with one-dimensional (1D), two-dimensional (2D) and three-dimensional (3D) morphologies of silver nanoparticles in Choline bis(trifluromethylsulfonyl)imide ([Choline][NTf_2]) IL. The 1D, 2D, and 3D silver nanoparticles were nanowires, nanoplates, and nanospheres respectively. The effect of nanoparticles morphology on density, viscosity and thermal conductivity of silver nanofluids (NF's) and silver IoNanoFluids were studied to explore the role of nanoparticles morphology on heat transfer properties of NF's and INF's.

2. EXPERIMENTAL DETAILS

2.1. Materials

Choline bis(trifluoromethylsulfonyl)imide (CAS No 827027-25-8) brought by Iolitec, 50 nm econix silver nanospheres (Lot# DAC 1296-MGM2091B) provided by nanoComposix, Inc. USA, 550 nm resonant silver nanoplates (Lot# KJW2047) supplied by nanoComposix, Inc. USA, silver nanowires 50 nm width and length of 50 μm procured from EMFUTUR company Europe, were used without further purification. Also, Millipore water (resistivity lower than 18.2 M$\Omega \cdot$cm) was used to formulate the NF's.

2.2. Preparation of Silver Nanofluids (Ag-NF's) and Silver IoNanoFluid (Ag-INF's)

To prepare silver nanofluids of nanowires and nanospheres morphologies, 0.002 g of silver nanoparticles were added into 100 mL of Millipore water. Then, this solution was sonicated for 20 minutes to obtain a homogeneous dispersion of silver nanoparticles in water. Silver nanoplates were readily available in dispersion form in water with the same concentration for other NF's.

Ag-INF's with various morphologies (nanowires, nanoplates and nanospheres) were prepared in [Choline][NTf_2] IL as a base fluid. First an equal amount of IL and the previously prepared silver nanoparticles based NF's were mixed together in a conical flask. The mixture forms two layers, a viscous layer of IL at the bottom and another immiscible layer above it. The mixture was then transferred to a round-bottom flask. Afterword's, it was connected to a rota-evaporator to transfer the Ag nanoparticles from the water phase to the ionic liquid phase. This mixture was heated at 80 °C for four hours to evaporate the water from the mixture. The remaining water was removed by drying on a vacuum line for two days to obtain dry Ag-INF's.

2.3. Characterization and Measurement of Heat Transport Properties

^{1}H and ^{13}C Nuclear magnetic resonance (NMR) spectra of samples were recorded on a Varian 400 spectrometer operating at 400 MHz. For NMR analysis, approximately 10 mg of the sample was taken into 2 mm NMR tube and samples were dispersed in a $CDCl_3$ solvent. Tetramethylsilane (TMS) was used as an internal reference for NMR chemical shift. The water content of [Choline][NTf_2] and Ag-INF's samples was measured with a Karl-Fischer coulometer (Mettler Toledo, mod. C20). The water content was found to be 30 ppm to 60 ppm before measurement. All Attenuated total reflection-infrared (ATR-IR) spectra of ILs, NF's and INF's were collected in a range from 600 cm^{-1} to 4000 cm^{-1} on an infrared spectrometer (Fourier Transform Jasco FT/IR-600 Plus). Optical absorptions of [Choline][NTf_2], Ag-NF's and Ag-INF's were measured with 8453 UV-Visible spectrophotometer. Optical data of samples were collected in a quartz cell. The cell was sealed with Teflon during the experiment to avoid moisture from the atmosphere. The thermal analysis of [Choline][NTf_2], Ag-NF's and Ag-INF's was done with a Mettler Toledo Thermal gravimetric analysis/Differential thermal analysis (TGA/DTA) (mod. 851) from 30 °C to 500 °C in nitrogen (N_2) atmosphere with a heating rate of 5 °C/min. The Scanning electron microscopy (SEM) analysis of Ag-NF's and Ag-INF's was carried out on a JEOL 6400 (20 kV) Scanning electron microscope. Elemental mapping analysis of silver IoNanoFluids was executed with a SEM JEOL 6400 + EDX Oxford instrument. The surface analysis of [Choline][NTf_2], Ag-NF's and Ag-INF's was completed with X-ray photoelectron spectroscopy (XPS) analysis on a V. G. Scientific, U. K. ESCA-3000 model. The sample preparation method was an identical method as applied before for the characterization of imidazolium halide ILs and ruthenium INF's.[18] TEM analysis of Ag-NF's and Ag-INF's was carried out using a TEM JEOL 1011 Transmission electron microscope (TEM) at an accelerating voltage of 100 kV. The density of the fluid samples was measured with an Anton Paar DSA 5000 densitometer. The density was measured within a temperature range from 293.15 K to 343.15 K. Viscosity was measured from 293.15 K to 343.15 K using a piston-type viscometer (Cambridge Visco-Pro 2000). Both devices were previously calibrated with density and viscosity reference fluids (S20 and S200, Koehler Instrument Company, Inc.).[20] Estimated expanded uncertainty ($k = 2$) was 1 kg/m^3 for density, 0.05 mPa$\cdot$s for viscosity and 0.1 K for temperature. The thermal conductivity of IL's and INF's was measured from 293.15 K to 333.15 K using a Thermal properties analyzer (Decagon Devices, Inc., mod. KD2 Pro), previously calibrated with glycerin. Expanded uncertainty ($k = 2$) was estimated lower than 5%

ARTICLE

of the thermal conductivity value[a] and 0.2 K for temperature. The thermophysical properties of all fluid samples were measured at atmospheric pressure.

3. RESULTS AND DISCUSSION

3.1. Structural Analysis

The structure of IL used in this study is presented in Figure 1. The structure of Choline bis(triflurometh-ylsulfonyl)imide was characterized by ^{1}H and ^{13}C NMR spectroscopy to ensure the purity of procured ionic liquid.

The structural variation in ILs after interactions with 1D, 2D, and 3D nanoparticle surfaces of silver in base IL was studied with ^{1}H and ^{13}C NMR analysis. Peak assignments observed for samples through ^{1}H and ^{13}C NMR analysis are shown in Figures 2 and 3. The obtained ^{1}H NMR peak assignments for [Choline][NTf_2] are in good agreements with the literature data.[21] However, one peak at 3.41 ppm observed in the ^{1}H NMR spectrum was due to traces of water exist in an IL. The peak obtained at 5.23 ppm of hydroxyl proton (–OH) in ^{1}H NMR spectrum was disappeared in all silver-IoNanofluid (Ag-INF's) samples (Fig. 2).

Obtained NMR assignments in NMR spectrum in Figure 2 reveal that hydroxyl (–OH) group from IL cation has an interaction with Ag nanoparticles in the case of all three Ag-INF's. This means that (–OH) proton from ionic liquid counterparts plays a decisive role in the solvation and stabilization of Ag-nanoparticles dispersion in the IL medium derived from the aqueous medium. All neat NMR spectral assignments to base ionic liquid and Ag-INF's are shown in Table I. For the ^{13}C NMR analysis of fluid samples no structural variation observed for the IL structure after interaction with silver nanoparticles in IL medium (Fig. 3).

3.2. UV-Visible Absorption Study

The UV-Visible absorption spectra of [Choline][NTf_2], Ag-NF's and Ag-INF's with three different geometries (nanowires, nanoplates and nanospheres) are shown in Figure 4. The UV-Visible absorption spectra of all Ag-NF's and Ag-INF's samples were recorded without further dilution. UV-Visible characterization gives useful information about their structures which depends on their size, shapes, and dielectric functions.[22] Silver nanowires dispersion in H_2O as a solvent shows a sharp peak at 377.10 nm and another broad peak at 758.75 nm (Fig. 4(a)). It is well known that metal nanoparticles have localized surface plasmon resonance (LSPR) due to the coherent oscillation of conduction electrons on the surface of metal nanoparticles in resonance with the electromagnetic waves at the metal-dielectric interface.[23, 24]

[a]This number can increase up to 10% for the liquids with low viscosity values (less than 20 mPa·s), which happens to most of the ionic liquids at high temperatures.

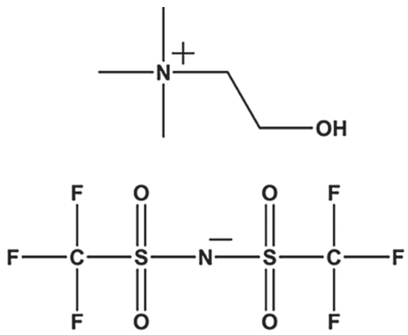

Fig. 1. Chemical structure of choline bis(triflurometh-ylsulfonyl)imide ionic liquid.

The Surface Plasmonic Resonance (SPR) peak for silver nanoparticles is usually observed at 400 nm. However, absorption of silver nanoparticle colloids fluctuates with the disparity of particle size and morphology.[25] The sharp peak at 377.10 nm has revealed a blue shift from 400 nm SPR peak of silver for nanowires morphology. The next broad optical absorption observed at 758.57 nm is for the hyperbranched structures of Ag-Nanowires.[26] This observation evidently witnesses in SEM and TEM micrographs for Ag-Nanowires-NF in Figures 8 and 9. Ag-Nanoplates-NF has two distinct optical absorptions, among them one at 399.50 nm due to SPR absorption of silver and corresponds to the out-of-plane quadruple mode of Ag-Nanoplates.[27] The peak at 555.00 nm attributed to in-plane dipolar SPR modes of resonant silver nanoplates.[27] Ag-Nanospheres-NF spectrum illustrates absorption maximum at 421.00 nm which solely depend on the particle size of Ag-Nanospheres.[28] The UV-Visible optical absorption study of INF's containing silver nanowires, nanoplates and nanospheres were performed to observe the surface modification of silver nanoparticles after their transfer from water medium to IL solvent medium. Optical absorption of [Choline][NTf_2] was studied as a control. Choline cation does not have any aromatic character or conjugation. Furthermore [NTf_2] anion does not have any chromophores in the structure, it results in no absorption for IL in the UV-Visible region.[25] Also, evident from the no color for [Choline][NTf_2] IL in Figure 5.

The UV-Visible absorptions were more shifted towards the red shift after the dispersion of silver nanoparticles from the aqueous phase to IL phase. This transformation leads to the color change of 1D, 2D, and 3D silver nanoparticles. Ag-Nanowires-NF, Ag-Nanoplates-NF and Ag-Nanospheres-NF had transparent white, resonant blue and yellow colors respectively. However, after nanoparticles dispersion in IL medium, they vary colors as turbid white, faint black and faint yellow for 1D, 2D, and 3D Ag-INF's. Color variation of Ag-NF's and Ag-INF's can be clearly observed in Figure 5. In the case of all three Ag-INF's which have the same concentration of silver nanoparticles (0.02 mg/mL) shows peaks broadening and

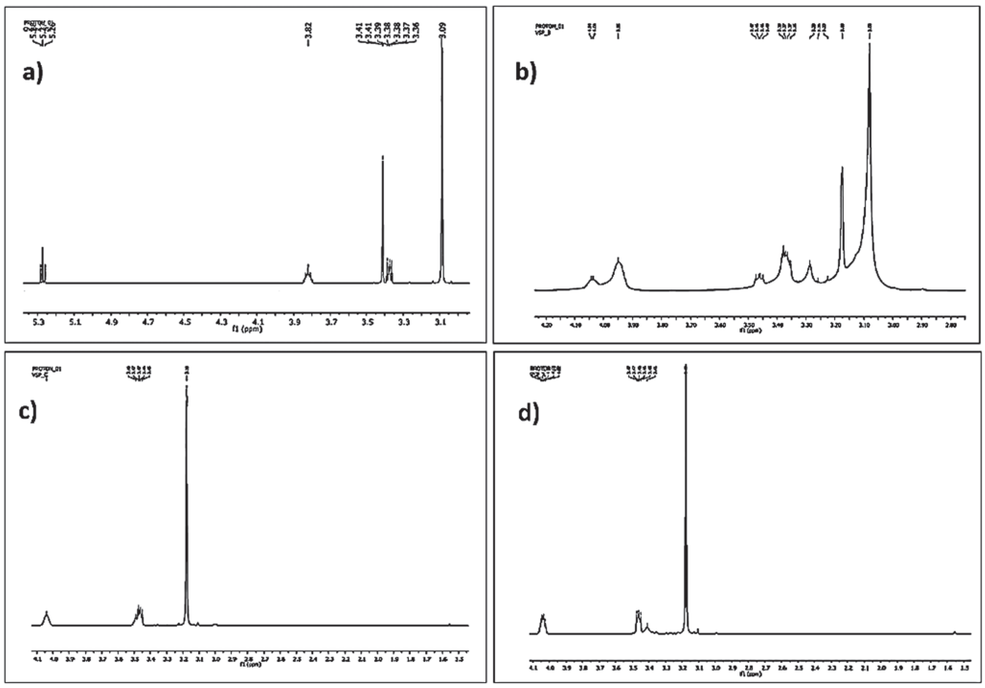

Fig. 2. ^{1}H NMR spectrum of (a) [Choline][NTf_2] IL, (b) Ag-Nanowires-INF, (c) Ag-Nanoplates-INF, (d) Ag-Nanospheres-INF.

shifts towards longer wavelength (red shift) due to growth in particle size.[29] It is a cause of single layer coating of dense viscous IL medium on the surface of nanoparticles. It also evident from the SEM and TEM micrographs from Figures 8 and 9.

3.3. Thermal Stability Study

Nowadays, metal nanoparticle in conventional solvents like water becomes a point of attention for the scientific community due to advantages such as reduced pumping power and enhanced heat conduction in heat transfer

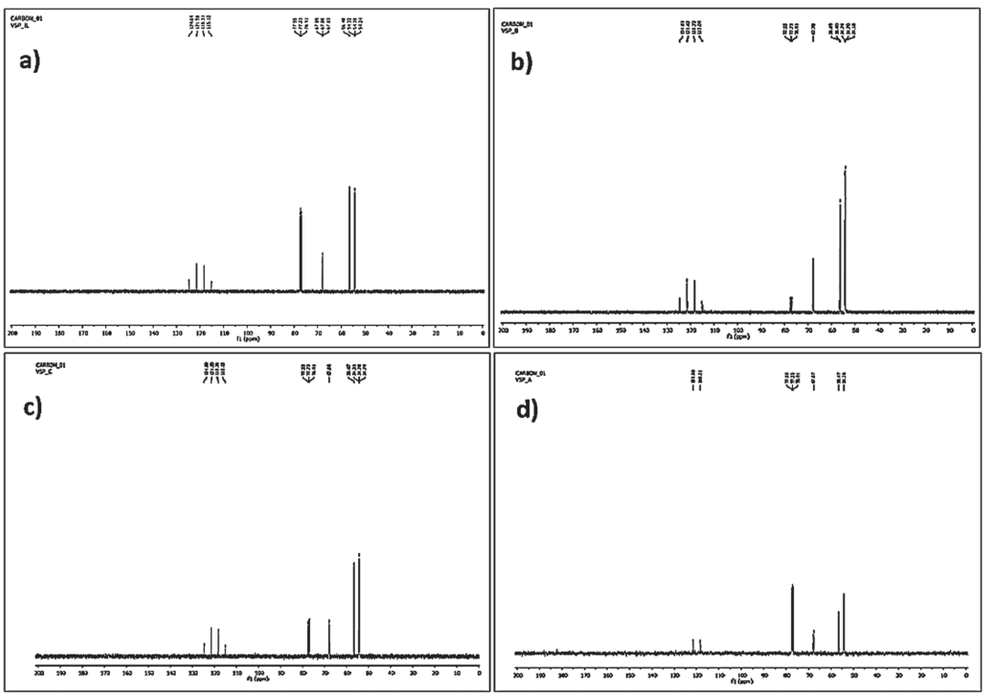

Fig. 3. ^{13}C NMR spectrum of (a) [Choline][NTf_2] IL, (b) Ag-Nanowires-INF, (c) Ag-Nanoplates-INF, (d) Ag-Nanospheres-INF.

Table I. ^{1}H and ^{13}C NMR assignments for [Choline][NTf_2] IL and Ag-INF's.

Sample name	^{1}H and ^{13}C NMR spectroscopy (400 MHz $CDCl_3$) (shift ppm)
[Choline][NTf_2]	^{1}H NMR: 3.09 (s, 6H, $N(CH_3)_3$, $-CH_2-CH_2-OH$), 3.37 (*t*, 2H, $N(CH_3)_3$, $-CH_2-CH_2$ OH), 3.82 (*m*, 2H, $N(CH_3)_3$, $-CH_2-CH_2-OH$), 5.27 (*t*, 1H, $N(CH_3)_3$, $-CH_2-CH_2-OH$)
	^{13}C NMR: 54.28 (*s*, 6H, $N(CH_3)_3$, $-CH_2-CH_2-OH$), 67.86 (*s*, 2H, $N(CH_3)_3$ $-CH_2-CH_2$ OH), 56.48 (*s*, 2H, $N(CH_3)_3$, $-CH_2-CH_2-OH$)
Ag-Nanowires-INF	^{1}H NMR: 3.18 (*s*, 6H, $N(CH_3)_3$, $-CH_2-CH_2-OH$), 3.46 (*t*, 2H, $N(CH_3)_3$ $-CH_2-CH_2$ OH), 4.04 (*m*, 2H, $N(CH_3)_3$, $-CH_2-CH_2-OH$)
	^{13}C NMR: 54.20 (*s*, 6H, $N(CH_3)_3$, $-CH_2-CH_2-OH$), 67.78 (*s*, 2H, $N(CH_3)_3$ $-CH_2-CH_2$ OH), 56.49 (*s*, 2H, $N(CH_3)_3$, $-CH_2-CH_2-OH$)
Ag-Nanoplates-INF	^{1}H NMR: 3.18 (*s*, 6H, $N(CH_3)_3$, $-CH_2-CH_2-OH$), 3.47 (*t*, 2H, $N(CH_3)_3$ $-CH_2-CH_2$ OH), 4.05 (*m*, 2H, $N(CH_3)_3$, $-CH_2-CH_2-OH$)
	^{13}C NMR: 54.28 (*s*, 6H, $N(CH_3)_3$, $-CH_2-CH_2-OH$), 67.86 (*s*,2H, $N(CH_3)_3$ $-CH_2-CH_2$ OH), 56.47 (*s*, 2H, $N(CH_3)_3$, $-CH_2-CH_2-OH$)
Ag-Nanospheres-INF	^{1}H NMR: 3.18 (*s*, 6H, $N(CH_3)_3$, $-CH_2-CH_2-OH$), 3.47 (*t*, 2H, $N(CH_3)_3$ $-CH_2-CH_2$ OH), 4.05 (*m*, 2H, $N(CH_3)_3$, $-CH_2-CH_2-OH$)
	^{13}C NMR: 54.28 (*s*, 6H, $N(CH_3)_3$, $-CH_2-CH_2-OH$), 67.87 (*s*, 2H, $N(CH_3)_3$ $-CH_2-CH_2$ OH), 56.47 (*s*, 2H, $N(CH_3)_3$, $-CH_2-CH_2-OH$)

technologies.[30] Figure 6 illustrates thermal stabilities of pure IL, Ag-NF's and Ag-INF's. The liquid range upper limit is usually defined by the onset temperature (T_{onset}) which is determined from the step tangent method.[31, 32] The onset temperature and the temperature at which the compound degrade totally ($T_{degradation}$) are shown in Table II.

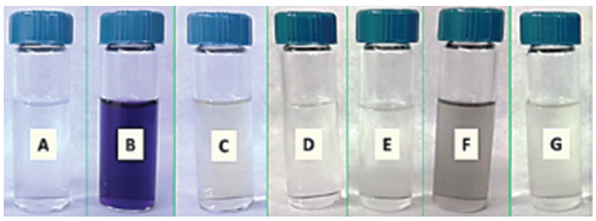

Fig. 5. Digital photography of (A) Ag-Nanowires-NF, (B) Ag-Nanoplates-NF, (C) Ag-Nanospheres-NF, (D) [Choline][NTf_2] IL, (E) Ag-Nanowires-INF, (F) Ag-Nanoplates-INF and (G) Ag-Nanospheres-INF.

The H_2O solvent based Ag-Nanowires-NF, Ag-Nanoplates-NF and Ag-Nanospheres-NF has similar trend and instability above 100 °C (Fig. 6). The various morphologies of Ag nanoparticles affect effectively for the thermal stability of NF's, following the trend Ag-Nanowires-NF (1D) > Ag-Nanoplates-NF (2D) > Ag-Nanospheres-NF (3D). This means that the nanofluid containing 1D silver nanowires is more stable compared to nanofluids containing 2D and 3D silver nanostructures. ILs are well known for their thermal stability. From the thermal gravimetric analysis results, we observed the [Choline][NTf_2] was thermally stable up to 376.6 °C in the nitrogen environment. Even though the concentration of dispersed silver nanoparticles was same, due to *in-situ* interactions of nanoparticles and IL surfaces it demonstrates the alteration in thermal stability of base IL and Ag-INF's. IL and its corresponding INF's thermal stability observed in the trend as follows: Ag-Nanoplates-INF > Ag-Nanospheres-INF > [Choline][NTf_2] > Ag-Nanowires-INF. In the case of Ag-INF's and [Choline][NTf_2], The residue remained in a sample pan from 2–5 weight% which was not degraded near to 400 °C, even though thermal scan was continued up to the 500 °C for Ag-INF's and [Choline][NTf_2]. Here we successfully demonstrated the significance of nanoparticle morphology on thermal stability. It becomes primarily important to study the effect of nanoparticle morphology on thermal stability when someone desires to use nanomaterials for high-temperature applications.[33] In another way, it is also revealed that slight

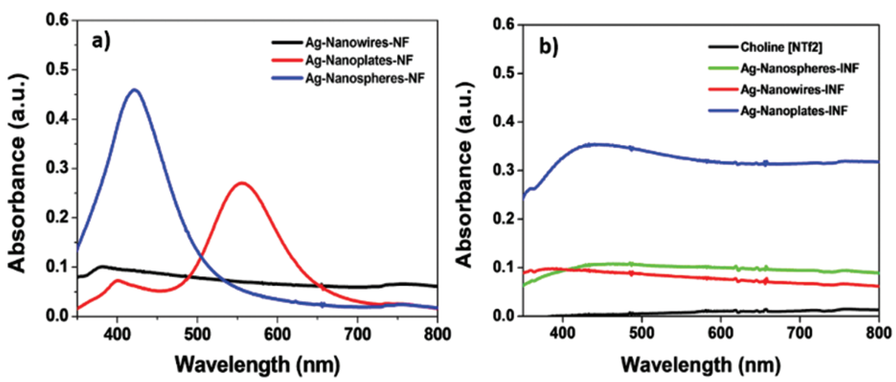

Fig. 4. UV-Visible absorption spectra of (a) Ag-NF's (b) [Choline][NTf_2] IL, and Ag-INF's with various geometries.

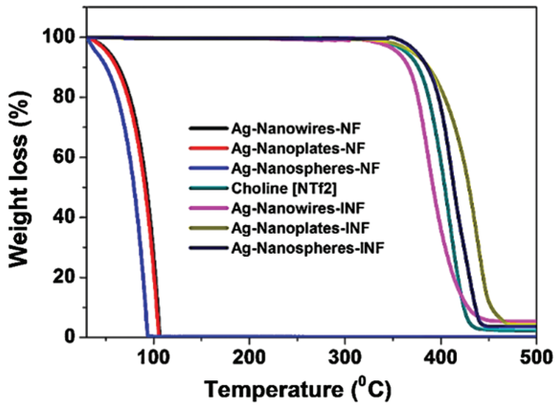

Fig. 6. Thermal gravimetric analysis of [Choline][NTf_2], Ag-NF's and Ag-INF's.

Table II. Thermal stability for pure IL, silver NF's and silver INF's in N_2 atmosphere.

Sample name	T_{onset} (°C)	$T_{degradation}$ (°C)
[Choline][NTf_2]	376.6	428.0
Ag-Nanowires-NF	74.7	106.7
Ag-Nanoplates-NF	70.4	104.2
Ag-Nanospheres-NF	59.7	93.8
Ag-Nanowires-INF	365.2	430.4
Ag-Nanoplates-INF	399.0	460.0
Ag-Nanospheres-INF	391.6	443.6

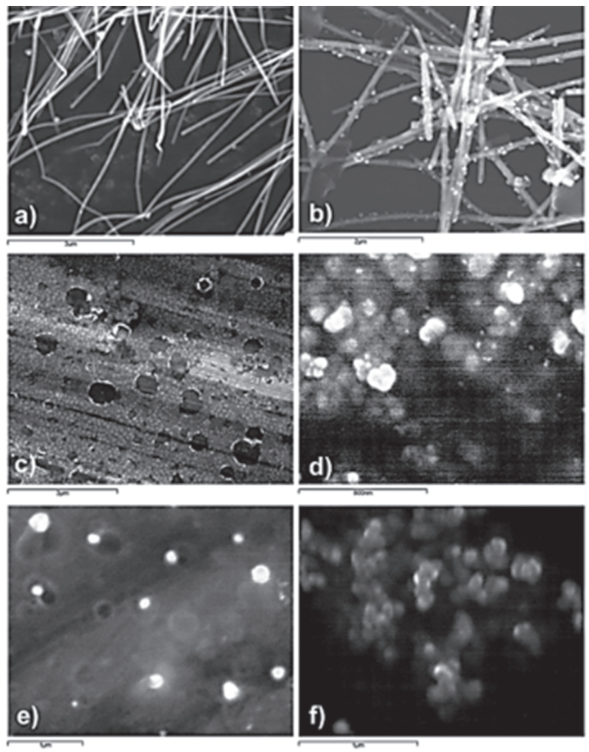

Fig. 8. SEM micrography of (a) Ag-Nanowires-NF, (b) Ag-Nanowires-INF, (c) Ag-Nanoplates-NF, (d) Ag-Nanoplates-NF, (e) Ag-Nanospheres-NF, and (f) Ag-Nanospheres-NF.

modification in nanoparticle surface also affects the thermal stability of nanoparticle dispersed fluids. The observed thermal stability was different for fluids having water and IL as a solvent. This is due to the surface interaction of 1D, 2D and 3D nanoparticle surfaces with [Choline][NTf_2] IL surface.

3.4. Infrared Spectroscopy Study

The effect of silver nanoparticles morphologies on bonding of Ag-NF's and Ag-INF's was studied with the ATR-IR technique (Fig. 7(a)). The sharp peak obtained at 1638 cm^{-1} (Fig. 7(a)) was originated from silver nanoparticles stabilized by polyvinylpyrrolidone (PVP) stabilizer. Giri et al. reported the single peak at 1645 cm^{-1} in the case of PVP nanosilver matrix.[29] We observed the peaks at 1638 cm^{-1} and in the range of (3200–3500 cm^{-1}) for all Ag-NF's with the different morphologies because nanoparticles were dispersed in water.[34] For the [Choline][NTf_2] the peak at 3550 cm^{-1} was assigned to the hydroxyl group present in Choline cation. The Ag-Nanowires-INF

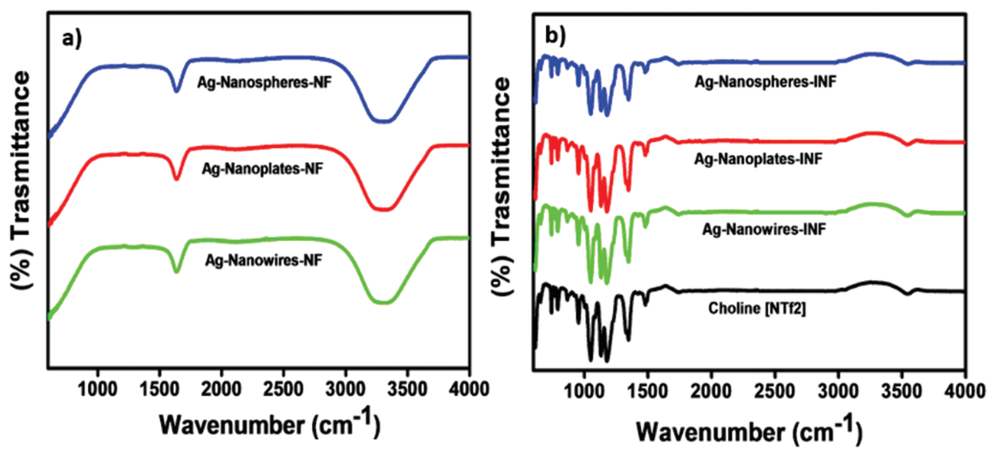

Fig. 7. ATR-IR spectra of (a) Ag-NF's, (b) [Choline][NTf_2]IL and Ag-INF's.

and Ag-Nanospheres-INF, displays a peak shift towards 3545 cm^{-1} and the same peak at 3540 cm^{-1} attributed for Ag-Nanoplates-INF. The results are consistent with ^{1}H NMR results of silver INF's (Fig. 2). Both results disclose hydroxyl group from Choline cation has an essential role in stabilization and dispersion of silver nanoparticles in IL medium. The common peaks for IL and INF's at 1476 cm^{-1} and 737 cm^{-1} were due to a small structural chain of alkane existing in choline cation. The peaks observed at 1174 cm^{-1}, 1132 cm^{-1}, and 1048 cm^{-1} (Fig. 7(b)) are attributed to C–N stretch, and those at 657 cm^{-1} and 867 cm^{-1} are assigned to C–F stretch present in $[NTf_2]$ anion.

3.5. Scanning Electron Microscopy Study

Figure 8 displays Scanning electron micrographs of the commercially purchased Ag-NF's with three diverse morphologies in water and $[Choline][NTf_2]$ solvents.

3.6. Transmission Electron Microscopy Analysis

For TEM analysis, Ag-Nanofluids were diluted in 3 mL of Millipore water and Ag-IoNanofluids solutions were diluted in 3 mL of acetone. The above dispersions were dropped on a carbon-coated copper grid. The sample spread on the TEM grid was dried at room temperature for 24 hours. Ag-Nanowires displayed good dispersion in water (Fig. 9(a)), nevertheless when they were dispersed in IL (Fig. 9(b)) the diameter of Ag-Nanowires observed was lower than in NF's. Ag-Nanoplates-NF (Fig. 9(c)) had very good dispersion but the sizes vary in the range of 30 to 50 nm. This may be the reason of ultra-sonication used for dispersing the nanoparticles in solvents. In the Ag-Nanoplates-INF, the nanoplates were agglomerated (Fig. 9(d)), which consequences in a further red shift of Ag-Nanoplates-INF in the UV-Visible spectrum (Fig. 4(b)). For Ag-Nanospheres in water and $[Choline][NTf_2]$ (Figs. 9(e, f)), the silver nanospheres were observed to be well dispersed in both solvents. The three-dimensional Ag-Nanospheres were observed as embedded particles in an ionic liquid media (Fig. 9(f)). The SEM (Fig. 8) and TEM (Fig. 9) analysis divulge that 1D, 2D and 3D nanostructures can be successfully transferred from water solvent to IL solvent.

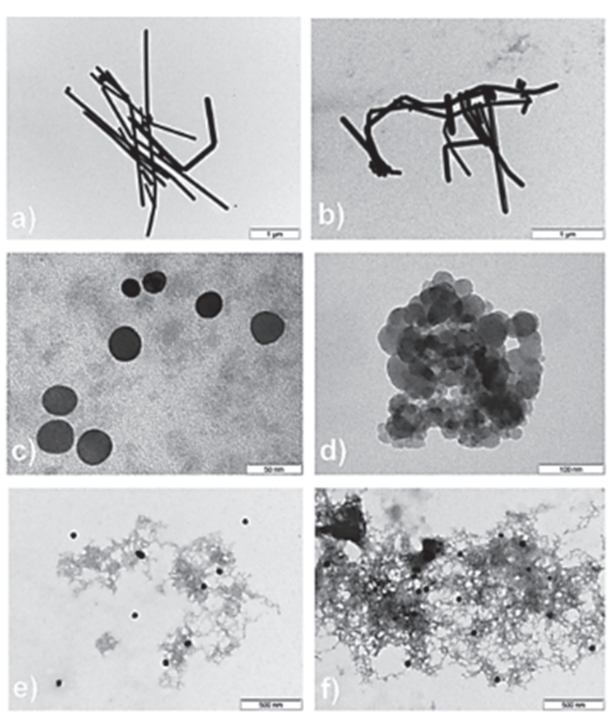

Fig. 9. TEM micrograph of (a) Ag-Nanowires-NF, (b) Ag-Nanowires-INF, (c) Ag-Nanoplates-NF, (d) Ag-Nanoplates-INF, (e) Ag-Nanospheres-NF and (f) Ag-Nanospheres-INF.

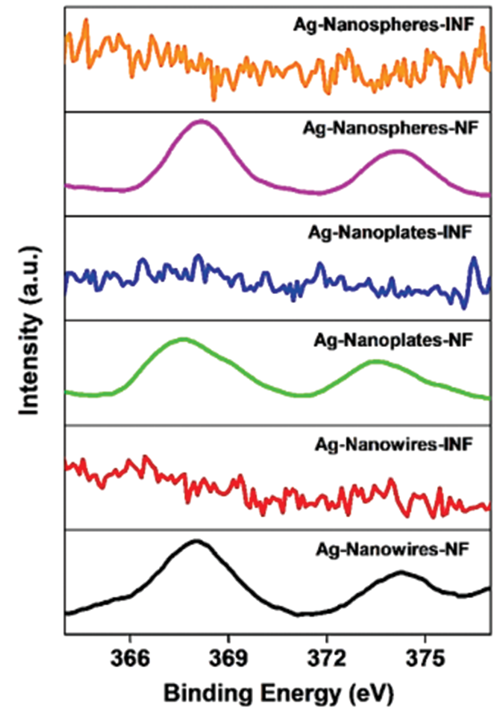

Fig. 10. XPS spectrum of Ag 3*d* for Ag-NF's and Ag-INF's.

3.7. X-ray Photoelectron Spectroscopy and Energy Dispersive Analysis

The electronic environment of silver nanoparticles with various morphologies in water and IL solvents were studied with X-ray photoelectron spectroscopy (XPS). The samples were mounted by drop casting on the XPS sampling stud. After, the sample mounting, it was immediately introduced into the high vacuum chamber of XPS. The samples

Table III. Binding energy assignments for silver nanofluids.

Sample	$3d_{5/2}$ (eV)	$3d_{3/2}$ (eV)
Ag-Nanowires-NF	368.01	374.31
Ag-Nanoplates-NF	367.62	373.52
Ag-Nanospheres-NF	368.02	374.20

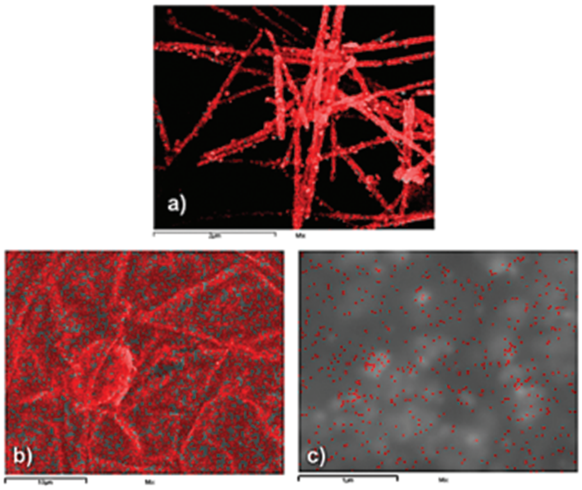

Fig. 11. EDS mapping of (a) Ag-Nanowires-INF, (b) Ag-Nanoplates-INF and (c) Ag-Nanospheres-INF.

were scanned for the detection of Ag metal within a binding energy of (361–379 eV). XPS spectra of Ag 3*d* for Ag-NF's and Ag-INF's are demonstrated in Figure 10.

The high-resolution XPS spectrum displays binding energy positions for Ag $3d_{5/2}$ and Ag $3d_{3/2}$ peaks for silver. Obtained peak positions predict the presence of silver nanoparticles in H_2O and IL solvents from Table III. For the Ag-INF's dispersions, a metal surface was fully covered with a thin layer of an ionic liquid. Since the analyzing X-rays do not reach to the silver metal surface it outcomes into the absence of Ag peaks in Ag-INF's XPS spectrum. Hence, to confirm the presence of silver nanoparticles in Ag-INF's, we employed Energy Dispersive Analysis (EDS) technique to map the existing silver. The EDS analysis detected the presence of silver nanoparticles in all three Ag-INF's samples (Fig. 11). The acquired results ensured the successful transfer of silver nanoparticles from the water phase to the IL phase.

4. EFFECT OF SILVER NANOPARTICLES MORPHOLOGY ON THERMOPHYSICAL PROPERTIES

A water impurity has an adverse effect on thermophysical properties of ILs and INF's.[14] For this reason, all samples were vacuum dried for 2 days prior to measurements. The water content of samples was determined with a Karl-Fisher titration coulometer, before and after of each measurement. Table IV shows the water contents of ILs and INF's samples before and after measurements. It can be observed from the table, the samples absorb water during the experiment.

4.1. Effect of Silver Nanoparticles Morphology on Density

The density of the samples was measured at atmospheric pressure, from 293.15 K to 343.15 K. Each nanofluid sample contains an equal amount of silver nanoparticles, were dispersed in an equal amount of solvent for the comparison of their influence on density. The density of all fluids studied were decreased when the temperature increases as evident from the Figure 12.

It was observed that Ag-Nanowires-NF which is one dimensional in nature experience less compactness between nanoparticle surfaces, outcomes a decrease in the density compared to 2D and 3D morphologies (Fig. 12(a)). Ag-Nanoplates-NF (2D morphology) demonstrates the highest density. To study the effect of nanoparticles morphology after addition in IL solvent, we first measured the density of dried [Choline][NTf_2] IL. The density of [Choline][NTf_2] IL and Ag-INF's not illustrated any considerable impact on density relate to variation in nanoparticles morphology (Fig. 12(b)). The obtained density results for each measured liquid were fitted with temperature according to Eq. (1). The relative deviation and Root-mean-square deviation (RMSD%) were calculated with the Eqs. (2) and (3), and they are presented in Table VI.

$$\rho/\mathrm{kg\cdot m^{-3}} = A_0 + A_1 \cdot (T/K) \quad (1)$$

$$\delta = 100 \cdot \left(\frac{X_e - X_c}{X_c}\right) \quad (2)$$

$$\mathrm{RMSD\%} = 100 \cdot \sqrt{\sum_N \frac{((X_c - X_e)/X_e)^2}{N}} \quad (3)$$

Table IV. Water content before and after measurement, for all the samples.

Sample name	Property	Water content before measurement (ppm)	Water content after measurement (ppm)
[Choline][NTf_2]	Density	51	747
Ag-Nanowires-INF		36	765
Ag-Nanoplates-INF		66	744
Ag-Nanospheres-INF		43	847
[Choline][NTf_2]	Viscosity	48	785
Ag-Nanowires-INF		31	799
Ag-Nanoplates-INF		39	736
Ag-Nanospheres-INF		42	801
[Choline][NTf_2]	Thermal conductivity	37	647
Ag-Nanowires-INF		30	793
Ag-Nanoplates-INF		35	734
Ag-Nanospheres-INF		41	888

Table V. Density of (kg/m^3) for pure IL, Ag-NF's and Ag-INF's at atmospheric pressure and from 293.15 K to 343.15 K.

T/K	293.15	303.15	313.15	323.15	333.15	343.15
[Choline][NTf_2]	1533.4	1523.9	1514.4	1505.1	1496.0	1486.9
Ag-Nanowires-NF	998.2	995.6	992.2	988.0	983.2	977.0
Ag-Nanoplates-NF	999.3	996.7	993.2	989.0	984.4	979.1
Ag-Nanospheres-NF	998.8	996.3	992.8	988.6	983.8	978.1
Ag-Nanowires-INF	1533.9	1523.1	1513.7	1504.4	1495.2	1486.1
Ag-Nanoplates-INF	1534.5	1524.9	1515.5	1506.2	1497.1	1488.0
Ag-Nanospheres-INF	1533.7	1524.2	1514.6	1505.3	1496.1	1487.1

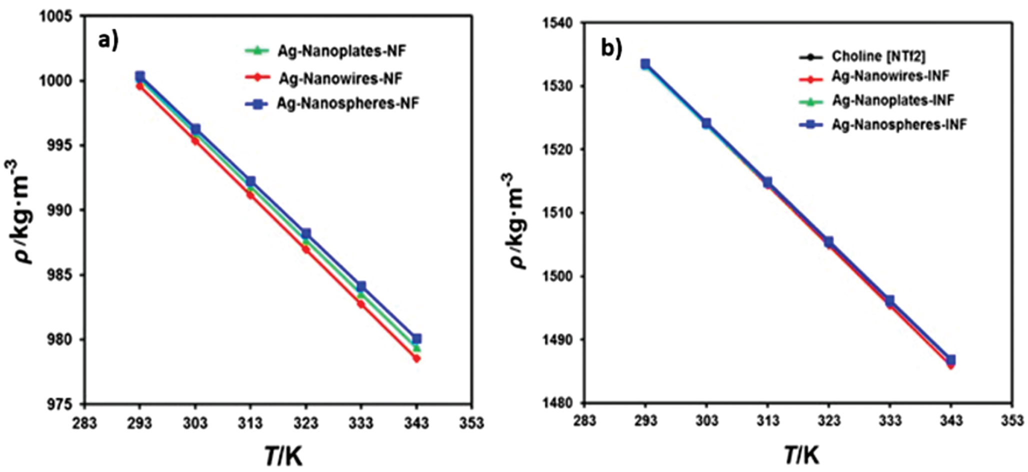

Fig. 12. Density of (a) Ag-NF's and (b) IL and Ag-INF's with various morphologies from 293.15 K to 343.15 K at atmospheric pressure.

X_c = the calculated value using the correlation, X_e = the experimental value and N is the total number of values compared.

The obtained density values for the IL ([Choline][NTf_2]) were compared with literature values. We found only one reference in the literature for a density measurement of [Choline][NTf_2] IL for the same technique used by us.[35] The reported values of density for base IL in the temperature range of 293.15 K to 343.15 K shows the maximum deviation of 0.17% compared to our data at 313.15 K. It could be the impact of traces of water impurities.[14] We provided details of the water content of ionic liquid and IoNanofluid samples before and after measurement in Table IV.

4.2. Effect of Silver Nanoparticles Morphology on Viscosity

The viscosity of Ag-NF's and Ag-INF's was measured in the temperature range from 293.15 K to 343.15 K. Table VII shows the viscosity values for all studied fluid samples.

Ag-NF's achieved very low viscosity, for all three samples (Fig. 13(a)). However, it was observed that all Ag-INF's have high viscosity due to viscous nature of the base ionic liquid. Ag-Nanowires-INF and Ag-Nanospheres-INF show similar viscosities with negligible difference. The IL and Ag-Nanoplates-INF have the highest viscosity. In both cases, viscosity could not be measured at 293.15 K, since their viscosities were out of range of our instruments. TEM micrograph obtained for Ag-Nanoplates-INF also reflects the agglomeration of silver nanoplates. It affects in the increase of viscosity for Ag-Nanoplates-INF (Fig. 8(d)).

$$\ln \eta/\text{mPa}\cdot\text{s} = A_0 + \frac{A_1}{T/K + A_2} \tag{4}$$

The viscosity values were correlated with temperature by the three-parameter Vogel Eq. (4). The (δ_{max}%), and root mean square deviation (RMSD%) were calculated according to Eqs. (2) and (3). The maximum deviation (δ_{max}%), and root-mean-square deviation (RMSD%) for the viscosity of each fluid are given in Table VIII.

We observed the reported value for the viscosity of [Choline][NTf_2] IL in the temperature range from 303.15 K to 343.15 K, had a maximum deviation with our data of 108% at 303.15 K.[35] This is since of traces of water impurities which have a considerable impact on thermophysical properties as described in an earlier report.[14]

4.3. Effect of Ag Nanoparticles Morphology on Thermal Conductivity

The thermal conductivity of Ag-NF's and Ag-INF's samples was measured at atmospheric pressure from 293.15 K to 333.15 K temperature range.

Table VI. Correlation parameters A_0 and A_1, maximum deviation (δ_{max} (%)), and root-mean-square deviation (RMSD(%)) for density.

Fluid	A_0/kg·m^{-3}	A_1/kg·m^{-3}K^{-1}	δ_{max}%	RMSD%
[Choline][NTf_2]	1805.800	−0.93	0.015	0.01
Ag-Nanowires-NF	1121.720	−0.4148	0.13	0.10
Ag-Nanoplates-NF	1123.000	−0.421	0.16	0.11
Ag-Nanospheres-NF	1119.400	−0.406	0.11	0.08
Ag-Nanowires-INF	1807.046	−0.933	0.02	0.01
Ag-Nanoplates-INF	1811.188	−0.948	0.05	0.03
Ag-Nanospheres-INF	1805.800	−0.93	0.09	0.08

Table VII. Viscosity for pure IL, Ag-NF's and Ag-INF's at atmospheric pressure 293.15 K to 343.15 K.

T/K	293.15	303.15	313.15	323.15	333.15	343.15
[Choline][NTf_2]	–	197	62.3	42.6	30.5	22.9
Ag-Nanowires-NF	1.03	0.70	0.65	0.55	0.49	0.40
Ag-Nanoplates-NF	1.05	0.81	0.66	0.55	0.45	0.40
Ag-Nanospheres-NF	1.03	0.80	0.63	0.51	0.43	0.38
Ag-Nanowires-INF	149	91.6	59.9	41.0	29.8	22.5
Ag-Nanoplates-INF	–	111	72.1	48.6	35.0	25.9
Ag-Nanospheres-INF	156	96.1	62.9	43.0	30.8	22.9

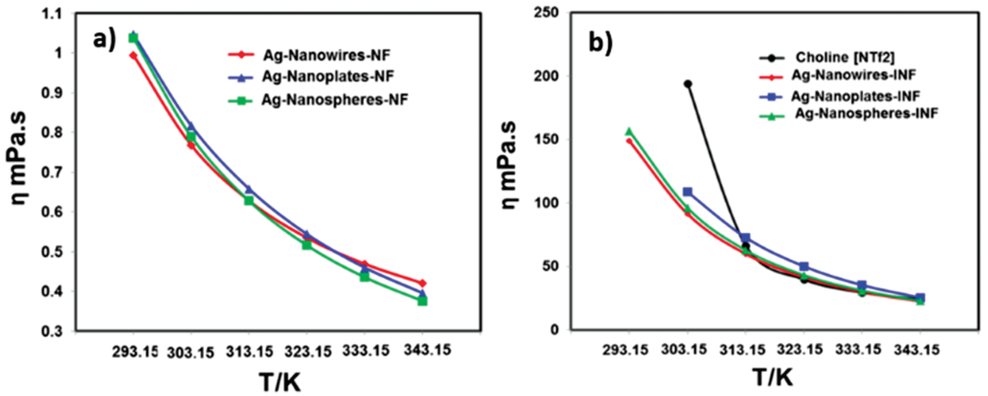

Fig. 13. Viscosity of (a) Ag-NF's and (b) IL and Ag-INF's with various morphologies from 293.15 K to 343.15 K at atmospheric pressure.

Table VIII. Correlation parameters A_0, A_1 and A_2, maximum deviation (δ_{max}%), and root-mean-square deviation (RMSD%) for viscosity.

Fluid	A_0	A_1/K	A_2/K	δ_{max}%	RMSD%
[Choline][NTf_2]	2.2328	55.42	−284.9	6.5	4.7
Ag-Nanowires-NF	−3.132	335.743	−187.2	1.3	1.1
Ag-Nanoplates-NF	−2.0635	142.963	−223.687	9.7	5.3
Ag-Nanospheres-NF	−3.558	487.331	−157.9	2.2	1.2
Ag-Nanowires-INF	−2.1	974	−157	0.40	0.2
Ag-Nanoplates-INF	−1.7493	864.71	−165.1	0.62	0.5
Ag-Nanospheres-INF	−6.865	3207.15	−25.56	2.9	1.7

Thermal conductivity for the Ag-NF's (Fig. 14(a)) is much greater than [Choline][NTf_2] IL and Ag-INF's (Fig. 14(b)). The Ag-Nanowires-NF sample has the highest thermal conductivity. The similar trend was observed for Ag-INF's in which Ag-Nanowires-INF displays higher thermal conductivity compared with other two Ag-INF's. After dispersion of silver nanoparticles in base ionic liquids, the enhancement in thermal conductivity was observed (Fig. 14(b)). The dependence with temperature is very remarkable in the case of the Ag-NF's, being observed a great enhancement of the thermal conductivity with temperature.

The thermal conductivity was correlated with temperature by the following equation.

$$\lambda/\mathrm{W}\cdot\mathrm{m}^{-1}\cdot\mathrm{K}^{-1} = A_0 + A_1 \cdot T/K \quad (5)$$

The obtained thermal conductivity results for each tested fluid were fitted to a straight line, according to Eq. (5). The relative deviation and Root-mean-square deviation (RMSD%) were calculated with the Eqs. (2) and (3). The coefficients obtained and root mean square deviations of the fits are provided in Table IX.

The same mass fraction addition of silver nanoparticles with three distinct morphologies in the same IL demonstrates variation in % enhancement of thermal conductivity in Ag-INF's. The % enhancement of thermal conductivity after addition of silver nanoparticles with 1D, 2D and 3D morphologies to base IL is given in Table XI.

There is no variation observed for the thermal conductivity of base IL ([Choline][NTf_2]) with variation in temperature from 293.15 K to 333.15 K. Enhancement in thermal conductivity was calculated with the formula $(\lambda_{INF}/\lambda_{IL} - 1)$. Where λ_{INF} represents thermal conductivity of IoNanofluid and λ_{IL} represents thermal conductivity of ionic liquid.[36]

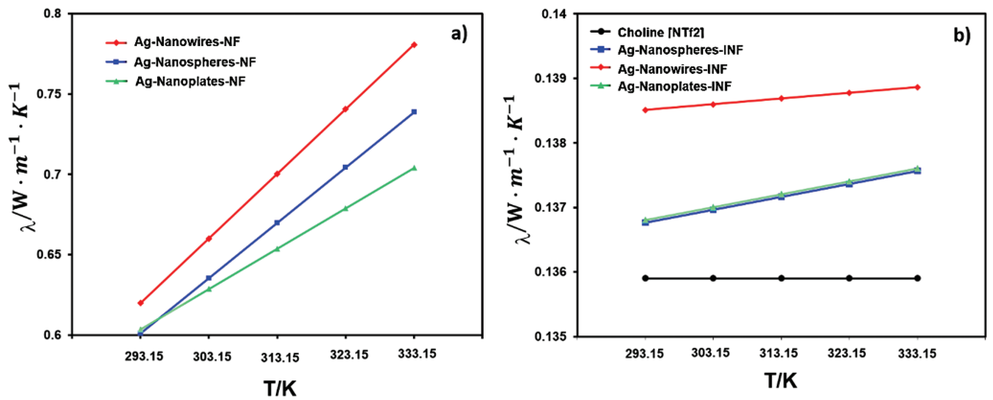

Fig. 14. Thermal conductivity of (a) Ag-NF's and (b) IL and Ag-INF's with various morphologies from 293.15 K to 333.15 K at atmospheric pressure.

ARTICLE

Table IX. Thermal conductivity for IL, Ag-NF's and Ag-INF's at atmospheric pressure from 293.15 K to 333.15 K.

T/K	293.15	303.15	313.15	323.15	333.15
[Choline][NTf_2]	0.136	0.136	0.136	0.136	0.136
Ag-Nanowires-NF	0.623	0.658	0.700	0.734	0.786
Ag-Nanoplates-NF	0.601	0.632	0.655	0.677	0.704
Ag-Nanospheres-NF	0.602	0.636	0.668	0.702	0.741
Ag-Nanowires-INF	0.136	0.137	0.138	0.140	0.142
Ag-Nanoplates-INF	0.137	0.137	0.137	0.137	0.138
Ag-Nanospheres-INF	0.137	0.137	0.137	0.137	0.138

Table X. Correlation parameters A_0 A_1 and A_2, maximum deviation (δ_{max}%), and root-mean-square deviation (RMSD%) for thermal conductivity.

Fluid	A_0/ $W \cdot m^{-1} \cdot K^{-1}$	$A_1 \cdot 10^5$/ $W \cdot m^{-1} \cdot K^{-2}$	δ_{max} (%)	RMSD (%)
[Choline][NTf_2]	0.1359	$-2.095 \cdot 10^{-5}$	0.32	0.22
Ag-Nanowires-NF	−0.4074	$3.44 \cdot 10^{-3}$	0.32	0.25
Ag-Nanoplates-NF	−0.5586	$4.02 \cdot 10^{-3}$	0.88	0.56
Ag-Nanospheres-NF	−0.1322	$2.51 \cdot 10^{-3}$	0.53	0.34
Ag-Nanowires-INF	0.1309	$2.0 \cdot 10^{-5}$	0.32	0.21
Ag-Nanoplates-INF	0.0982	$1.29 \cdot 10^{-4}$	0.58	0.34
Ag-Nanospheres-INF	0.13094	$2.0 \cdot 10^{-5}$	0.15	0.21

Compare to base IL, Ag-Nanospheres-INF shows 0.73% enhancement in thermal conductivity at all measured temperatures. The same trend was observed for the Ag-Nanoplates-INF which reflects 0.73% thermal conductivity enhancement from 293.15 K to 323.15 K. Ag-Nanoplates-INF had an enhancement of 1.47% thermal conductivity.

Table XI. Thermal conductivity ($W \cdot m^{-1} \cdot K^{-2}$) enhancement $(\lambda_{INF}/\lambda_{IL} - 1) * 100$ of Ag INF's.

Temperature (K)	Ag-Nanowires-INF	[Choline][NTf_2]	Enhancement (%)
293.15	0.136	0.136	0
303.15	0.137	0.136	0.73
313.15	0.138	0.136	1.47
323.15	0.140	0.136	2.94
333.15	0.142	0.136	4.41
Temperature (K)	Ag-Nanoplates-INF	[Choline][NTf_2]	Enhancement (%)
293.15	0.137	0.136	0.73
303.15	0.137	0.136	0.73
313.15	0.137	0.136	0.73
323.15	0.137	0.136	0.73
333.15	0.138	0.136	1.47
Temperature (K)	Ag-Nanospheres-INF	[Choline][NTf_2]	Enhancement (%)
293.15	0.137	0.136	0.73
303.15	0.137	0.136	0.73
313.15	0.137	0.136	0.73
323.15	0.137	0.136	0.73
333.15	0.138	0.136	0.73

However, Ag-Nanowire-INF thermal conductivity was varied at each temperature compared to base IL. This INF thermal conductivity enhancement observed from 0% to 4.41% for 293.15 K to 333.15 K temperatures respectively.

5. CONCLUSIONS

The hydroxyl functional group from Choline bis(trifluromethylsulfonyl)imide ionic liquid's interaction was detected with silver nanoparticle surface in ^{1}H NMR analysis. The Choline bis(trifluromethylsulfonyl)imide ionic liquid does not have optical absorption in UV-Visible range. The optical absorption of silver nanoparticles in H_2O and [Choline][NTf_2] IL were distinct from each other. The morphology of silver nanoparticles influences the absorption in UV-Visible for NF's and INF's. The water as a solvent limits the thermal stability of silver nanofluids however the IL as a solvent enhance the thermal stability of silver IoNanofluids. The Infrared spectroscopy study also proposes the interaction of hydroxyl functional group of IL to the silver nanoparticle surface. Silver nanoplates demonstrate the aggregation of plates during their transfer from H_2O to IL in Scanning electron microscopy and Transmission electron microscopy study. The silver nanoparticles surfaces covered with IL creates a barrier to detect silver in silver IoNanofluids by X-ray photoelectron spectroscopy. However, it is possible to detect silver nanoparticles with Energy dispersive analysis technique. The IoNanofluid having dispersed silver nanoplates had advanced viscosity due to agglomeration of nanoplates. There is no considerable effect of silver nanoparticle morphologies was observed on the density of INF's. The one-dimensional silver nanoparticles had highest thermal conductivity compared to two-dimensional silver nanoplates and three-dimensional silver nanospheres. This study will provide direction for the appropriate nanoparticles morphology selection in the designing of nanofluids and IoNanofluids for heat transfer fluid application.

LIST OF ABBREVIATIONS

1D: One-Dimensional.
2D: Two-Dimensional.
3D: Three-Dimensional.
IL: Ionic Liquid.
[Choline][NTf_2]: Choline bis(trifluoromethylsulfonyl) imide.
INF: IoNanofluid.
NF: Nanofluid.
Ag-NF: Silver Nanofluid.
Ag-INF: Silver IoNanofluid.
ATR-IR: Attenuated Total Reflection Infrared.
TGA: Thermal Gravimetric Analysis.
DTA: Differential Thermal Analysis.
SEM: Scanning Electron Microscopy.
TEM: Transmission Electron Microscopy.

NMR:	Nuclear Magnetic Resonance.
XPS:	X-ray Photoelectron Spectroscopy.
EDS:	Energy Dispersive Analysis.
UV-Visible:	Ultraviolet Visible.
OH:	Hydroxide
Ag-Nanowires-INF:	Silver Nanowires IoNanofluid.
Ag-Nanoplates-INF:	Silver Nanoplates IoNanofluid.
Ag-Nanospheres-INF:	Silver Nanospheres IoNanofluid.

Acknowledgments: This work was supported by the FP7-People-2010-IRSES Program (NARILAR-New Working Fluids based on Natural Refrigerants and Ionic Liquids for Absorption Refrigeration, Grant Number 269321).

References and Notes

1. L. Moens and D. M. Blake, Advanced heat transfer and thermal storage fluids, *Conference Paper*, January **(2005)**, NREL/CP-510-37083.
2. R. J. Bhatt, H. J. Patel, and O. G. Vashi, *IJRMET* 4, 16 **(2014)**.
3. J. Buongiorno, D. C. Venerus, N. Prabhat, T. McKrell, J. Townsend R. Christianson, Y. V. Tolmachev, P. Keblinski, L.-W. Hu, J. L. Alvarado, I. C. Bang, S. W. Bishnoi, M. Bonetti, F. Botz, A. Cecere, Y. Chang, G. Chen, H. Chen, S. J. Chung, M. K. Chyu, S. K. Das, R. D. Paola, Y. Ding, F. Dubois, G. Dzido, J. Eapen, W. Escher, D. Funfschilling, Q. Galand, J. Gao, P. E. Gharagozloo, K. E. Goodson, J. G. Gutierrez, H. Hong, M. Horton, K. S. Hwang, C. S. Iorio, S. P. Jang, A. B. Jarzebski, Y. Jiang, L. Jin, S. Kabelac, A. Kamath, M. A. Kedzierski, L. G. Kieng, C. Kim, J.-H. Kim, S. Kim, S. H. Lee, K. C. Leong, I. Manna, B. Michel, R. Ni, H. E. Patel, J. Philip, D. Poulikakos, C. Reynaud, R. Savino, P. K. Singh, P. Song, T. Sundararajan, E. Timofeeva, T. Tritcak, A. N. Turanov, S. V. Vaerenbergh, D. Wen, S. Witharana, C. Yang, W.-H. Yeh, X.-Z. Zhao, and S.-Q. Zhou, *J. Appl. Phys.* 106, 094312 **(2009)**.
4. J. Philip and P. D. Shima, *Adv. Colloid Interfac.* 183, 30 **(2012)**.
5. S. A. Angayarkanni and J. Philip, *J. Phys. Chem. C* 118, 13972 **(2014)**.
6. P. D. Shima and J. Philip, *Ind. Eng. Chem. Res.* 53, 980 **(2014)**.
7. S. A. Angayarkanni and J. Philip, *J. Appl. Phys.* 118, 094306 **(2015)**.
8. S. A. Angayarkanni, V. Sunny, and J. Philip, *J. Nanofluids* 4, 302 **(2015)**.
9. S. A. Angayarkanni and J. Philip, *Adv. Colloid Interfac.* 225, 146 **(2015)**.
10. H. A. Mintsa, G. Roy, C. T. Nguyen, and D. Doucet, *Int. J. Therm. Sci.* 48, 363 **(2009)**.
11. Y. Hwang, Y. Ahn, H. Shin, C. Lee, G. Kim, H. Park, and J. Lee, *Curr. Appl. Phys.* 6, 1068 **(2006)**.
12. D. Li, B. Hong, W. Fang, Y. Guo, and R. Lin, *Ind. Eng. Chem. Res.* 49, 1697 **(2010)**.
13. M. E. V. Valkenburg, R. L. Vaughn, M. Williams, and J. S. Wilkes, *Thermochim Acta* 425, 181 **(2005)**.
14. J. M. P. França, F. Reis, S. I. C. Vieira, M. J. V. Lourenço, F. J. V. Santos, C. A. Nieto de Castro, and A. A. H. Pádua, *J. Chem. Thermodyn.* 79, 248 **(2014)**.
15. N. Gathergood, M. T. Garcia, and P. J. Scammells, *Green Chem.* 6, 166 **(2004)**.
16. J. Bedia, J. Palomar, M. González-Miquel, F. Rodriguez, and J. J. Rodríguez, *Sep. Purif. Technol.* 95, 188 **(2012)**.
17. P. Warrier and A. Teja, *Nanoscale Res. Lett.* 247, 1 **(2011)**.
18. V. S. Patil, A. Cera-Manjarres, D. Salavera, C. V. Rode, K. R. Patil, C. A. Nieto De Castro, and A. Coronas, *J. Nanofluids* 5, 191 **(2016)**.
19. H. Xie, Z. Zhao, J. Zhao, and H. Gao, *Chin. J. Chem. Eng.* 24, 331 **(2016)**.
20. S. K. Chaudhari, D. Salavera, and A. Coronas, *J. Chem. Eng. Data* 56, 2861 **(2011)**.
21. A. J. Costa, M. R. Soromenho, K. Shimizu, I. M. Marrucho, J. M. Esperanca, J. N. Lopes, and L. P. Rebelo, *Chem. Phys. Chem.* 13, 1902 **(2012)**.
22. V. V. Vodanik, D. K. Bozanic, N. Bibic, Z. V. Saponjic, and J. M. Nedeljkovic, *J. Nanosci. Nanotechnol.* 8, 3511 **(2008)**.
23. G. Mie, *J. Ann. Phys.* 25, 377 **(1908)**.
24. V. M. Renteria and J. Garcia-Macedo, *Colloids Surf. A* 273, 1 **(2006)**.
25. F. Bian, X.-Z. Zhang, Z.-H. Wang, Q. Wu, H. Hu, and J.-J. Xu, *Chin. Phys. Lett.* 25, 4463 **(2008)**.
26. J. Zhang, C. S. Dayb, and D. L. Carroll, *Chem. Comm.* 6937 **(2009)**.
27. S.-W. Lee, S.-H. Chang, Y.-S. Lai, C.-C. Lin, C.-M. Tsai, Y.-C. Lee, J.-C. Chen, and C.-L. Huang, *Materials* 7, 7781 **(2014)**.
28. D. Paramelle, A. Sadovoy, S. Gorelik, P. Free, J. Hobleya, and D. G. Fernig, *Analyst* 139, 4855 **(2014)**.
29. N. Giri, R. K. Natarajan, S. Gunasekaran, and S. Shreemathi, *Archives of Applied Science Research* 3, 624 **(2011)**.
30. L. Cheng, *Recent Patents on Engineering* 3, 1 **(2009)**.
31. J. Restolho, J. L. Mata, and B. Saramago, *Fluid Phase Equilibr.* 322, 142 **(2012)**.
32. J. Salgado, M. Villanueva, J. J. Parajo, and J. Fernández, *J. Chem. Thermodyn.* 65, 184 **(2013)**.
33. E. Marzbanrad, G. Rivers, P. Peng, B. Zhaoac, and N. Y. Zhou, *Phys. Chem. Chem. Phys.* 17, 315 **(2015)**.
34. S. C. Manna, S. Mistria, and A. D. Jana, *Cryst. Eng. Comm.* 14, 7415 **(2012)**.
35. A. J. L. Costa, M. R. C. Soromenho, K. Shimizu, I. M. Marrucho, J. M. S. S. Esperança, J. N. C. Lopes, and L. P. N. Rebelo, *Chem. Phys. Chem.* 13, 1902 **(2012)**.
36. J. M. P. França, F. Reis, S. I. C. Vieira, M. J. V. Lourenço, F. J. V. Santos, C. A. Nieto de Castro, and A. A. H. Pádua, *J. Chem. Thermodynamics* 79, 248 **(2014)**.

ARTICLE